Dual-resolution coarse-grained simulation of the bisphenol-*A*-polycarbonate/nickel interface

Cameron F. Abrams,* Luigi Delle Site, and Kurt Kremer
Max-Planck-Institut für Polymerforschung, Ackermannweg 10, 55128 Mainz, Germany
(Received 19 September 2002; published 27 February 2003)

We present a dual-resolution coarse-graining scheme for efficient molecular dynamics simulations of bisphenol-*A*-polycarbonate (BP-*A*-PC) liquids in contact with a (111) nickel surface. The essential feature of this model is the strong adsorption of phenoxy chain ends, and the absence of adsorption by other parts of the chains. Details of how phenoxy chain ends interact with the nickel surface were extracted from Car-Parrinello molecular dynamics calculations of adsorption of phenol on nickel. These calculations show that phenol adsorption on nickel is short ranged (<3 Å) and strongly dependent on the C_1-C_4 orientation of the ring. The structure of BP-*A*-PC prevents internal phenylene groups from interacting with the surface, due to steric hindrances from the noninteracting isopropylidenes. These dependencies are incorporated in the coarse-grained model of the BP-*A*-PC chain by resolving chain-terminating carbonate groups with atomistic detail, while the rest of the chain is represented by coarsened ''beads.'' This allows specification of the C_1-C_4 orientation of the terminal phenoxy groups, while overall allowing for system equilibration with reasonable computer time. We simulate liquids of up to 240 chains of ten chemical repeat units, confined in a slit pore formed by two frozen (111) planes of atoms with the lattice spacing of nickel. We find that the strong adsorption of chain ends has a large effect on the liquid structure through a distance of more than two bulk radii of gyration from the surface. These effects are explained by a competition among single- and double-end adsorption, and dense packing. The structure of the interface less than 10 Å from the wall is greatly sensitive to the orientational dependence of the phenoxy adsorption.

DOI: 10.1103/PhysRevE.67.021807 PACS number(s): 36.20.Ey, 68.08.De

I. INTRODUCTION

Polymer simulations have recently often been used to study systematically coarse-grained molecular models [1–4]. Coarse-graining aims to guarantee that the chain conformations in a simulation sample represent true equilibrium conformations of the specific polymer considered. In principle, direct atomistic simulations of polymers could fulfill this requirement if the interatomic potential energy functions are reliable. In practice, however, this requirement is impossible to fulfill in atomistic simulations owing to limitations in computer power and characteristically long relaxation times for macromolecules. The global conformational relaxation takes (many) orders of magnitude more time than any local move. A central feature of coarse-graining is that the models retain only as much unique and relevant information as needed about the specific polymer(s) under investigation, using significantly fewer degrees of freedom (i.e., particles) than required for full atomistic detail. This also means that the characteristic time step in a simulation increases significantly. The coarsened degrees of freedom must be constrained within ensembles of configurations which represent an appropriate average over the microscopic atomic-scale potential energy surface for the fully resolved system. Once an equilibrated sample at the coarse-grained level is generated using an appropriate simulation technique which samples these ensembles, atomic details can be inverse mapped to study atomic-scale properties and processes on then appropriately short length and time scales [5].

Our focus in recent years has been to develop a method for coarse-graining melts of bisphenol-*A*-polycarbonate (BP-*A*-PC) [5–9] (Fig. 1). BP-*A*-PC not only provides a challenging test case for this type of modeling, it is also by far the most utilized and intensively studied variety of polycarbonate, thanks to its many valuable material properties, such as high impact strength, ductility, glass transition, and melting temperatures [10]. For example, interesting questions regarding the mechanisms of glassy BP-*A*-PC ductility have inspired many experimental [11–16], simulation [17–21], and combined experimental-simulation [22,23] studies. Such questions remain essentially unresolved, and certainly must involve both details of intermolecular packing and intramolecular conformations. Another interesting question is the origin of BP-*A*-PC's unusually small entanglement molecular weight M_e between six and seven of chemical repeat units [24]. Coarse-grained simulations can potentially fill a gap that now exists between traditional atomistic simulation and experiments, by addressing longer length and time scales, allowing one to test hypotheses regarding intermolecular and intramolecular interplay in packing and entanglement that are otherwise more difficult to approach.

For the purposes of this article, we are particularly inter-

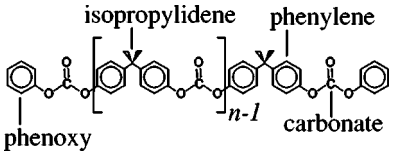

FIG. 1. Schematic representation of the structure of bisphenol-*A*-polycarbonate. The relevant comonomeric groups are labeled.

*Present address: Department of Chemical Engineering, Drexel University, Philadelphia, PA 19104. Electronic address: cfabrams@drexel.edu

ested in understanding the adhesion behavior of BP-*A*-PC liquids next to ideal metal surfaces. Metal surfaces are particularly relevant for industrial processing of polycarbonate, and indeed many other synthetic polymers. The interplay between specific local adsorption of organic chain segments and the much larger scale chain conformations is difficult to capture with traditionally simple molecular and atomic-scale models. Steps toward understanding this interplay, at least for systems of small single chains and structureless metal surfaces, have been taken. The influence of specific binding on aluminum on the conformational statistics of small oligomers of poly(methyl methacrylate) has been investigated [25–27]. We recently reported the development of a multiscale technique that handles both specific adsorption and global conformation of longer chains at the interface of a dense melt (the most relevant state for most kinds of polymer processing) and a metal surface [8]. This technique involved appropriate coupling of information from detailed *ab initio* calculations of small molecule–surface interactions into coarse-grained molecular dynamics simulations of liquids of comparatively much larger macromolecules. Here, we present a more complete account and the first set of refinements in the specificity of that model. The major refinement is the incorporation of an orientational dependence for the adsorption strength of chain-terminating phenoxy groups. As will be discussed, incorporating this dependence is key in predicting the interface structure and requires at a minimum *some* atomistic resolution. We have therefore constructed what we term a ''dual-resolution'' coarse-grained model of the BP-*A*-PC molecule, in which all parts of the chains *except for the ends* are represented by coarse-grained beads. Only the carbonate groups at the ends are resolved atomistically. To the best of our knowledge, this is the first such attempt at using a model with simultaneous coarse grained and atomistic resolution for molecular simulations of polymers.

Our paper is presented as follows. We first discuss the details of the dual-resolution BP-*A*-PC molecular model. We then discuss the simulation methods, including both the Car-Parrinello density functional theory (DFT) and coarse-grained simulations. Results of simulations of short BP-*A*-PC chains confined in a slit pore formed by two ideal nickel surfaces are then presented and discussed. Finally, the consequences of the results for the bulk surface coupling of the melt will be discussed.

II. THE DUAL-RESOLUTION COARSE-GRAINED MODEL OF BPA-PC

A. The single-resolution 4:1 model

Shown in Fig. 1 is the chemical structure of a BP-*A*-PC molecule composed of n repeat units. The general idea of coarse graining is to represent such a specific polymer molecule as a bead-spring chain, usually not explicitly accounting for internal structures of the repeat unit, such as phenyl rings and dangling methyl groups. The role of the beads is two fold: first, they must, as a group, reflect the proper conformational statistics of the given polymer, and second, they must exclude volume such that the molecule fills space and has a ''shape'' as close as possible to the given polymer molecule.

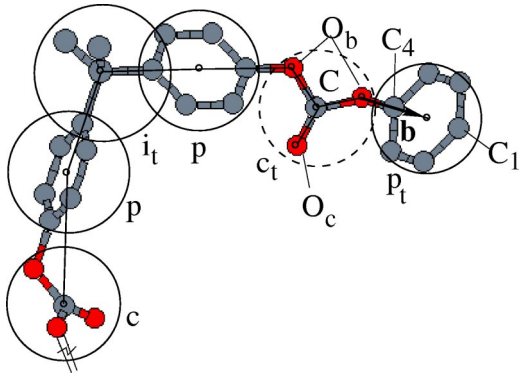

FIG. 2. Atomistic structure of a representative chain-end configuration of BP-*A*-PC, illustrating the dual-resolution scheme. The small black circles are mapping points in the scheme, and the large circles represent the excluded volume diameters of those points. The C_4-C_1 orientation vector **b** is shown. Lower-case letters denote coarse-grained bead designations: ''p'' is phenylene, ''c_t'' is the terminal carbonate, ''p_t'' is the terminal phenoxy, and ''i_t'' is the terminal isopropylidene. Capital letters denote atom type designations (see text).

The foundation of the dual-resolution model is our ''4:1'' coarse-graining scheme [9], which replaces each repeat unit of BP-*A*-PC by four beads. The beads loosely correspond to each of the four basic units of the repeat unit: an isopropylidene group, a carbonate group, and two linking phenylenes. For convenience, we label these bead types ''i'' for isopropylidene, ''c'' for carbonate, and ''p'' for phenylene. This allows us to represent the ends of the chains using the same types of coarse-grained beads, as depicted in Fig. 2.

Intramolecular constraining potentials are used to ensure that the conformations which the chains sample reflect the proper statistics given the atomic-scale potential energy surface. As the details behind this aspect of our technique were discussed previously [6], we present only a brief discussion here. These constraints take the form of bond angle potentials. For each carbonate-isopropylidene-carbonate (''c-i-c'') and isopropylidene-carbonate-isopropylidene (''i-c-i'') triple along a chain backbone, a potential $U(\theta)$ is used, which is a Boltzmann inversion of the corresponding probability density distribution for this type of angle. These probability distributions are defined by the respective coarse-grained mapping points on the chain's atomic structure and were generated via Metropolis Monte Carlo sampling of the conformations of a single atomistic chain in vacuum. Figure 3 shows these distributions for the case of $T=570$ K, a typical processing temperature for parity conservation. For the remainder of the discussion in the present paper, we use energy units of kT with $T=570$ K. Note that these types of triples are not formed by immediate neighbors along the backbone, because each i-c pair is bridged by a phenylene (''p'') bead. Note also that the mapping point of a phenylene bead never exactly corresponds to the center of a phenylene ring in the same way as the ispropylidene and carbonate mapping points correspond to subgroup centers in the atomic structure. This

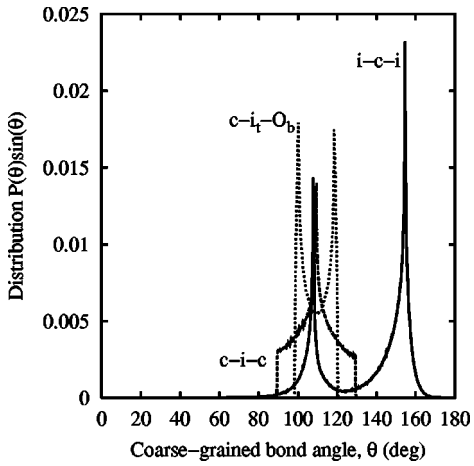

FIG. 3. Probability distributions for the coarse-grained bond angles: "*i*-*c*-*i*" (solid), "*c*-*i*-*c*" (long dash), "*c*-i_t-O_b" (short dash).

is because mapping a point to the exact center of each phenylene group introduces torsional degrees of freedom in the coarse-grained configurations, which are correlated to the bond angle degrees of freedom. To avoid this rather complicated situation, we "decouple" the phenylene mapping points from the centers of their respective atomic groups and enforce 180° bond angles. As discussed elsewhere, this adequately accounts for the excluded volume of the phenylenes in a dense melt of BP-*A*-PC [9].

Backbone bond angles at the phenylene beads (i.e., *i*-*p*-*c* bond angles) are enforced at 180° by a simple harmonic potential with a spring constant of $0.05kT/(\mathrm{deg})^2$. This constant reflects the combined effect of all four-body improper dihedrals used in atomistic simulations of molecules (e.g., bisphenol *A*) containing 1,4-phenylene moieties [21,29,30] Because phenylene beads which are immediate neighbors on either side of the same isopropylidene bead can weakly overlap, the excluded volume interaction for these intramolecular phenylene-phenylene pairs is turned off. This choice has a small effect on the resulting bond angle distributions around the isopropylidenes, a discussion of which appeared elsewhere [9]. Distances between neighboring beads are enforced with harmonic spring potentials [see Eq. (2) below]. Bonds between carbonates and phenylenes are enforced at 3.56 Å with a standard deviation of 0.04 Å, while bonds between isopropylidenes and phenylenes are enforced at 2.93 Å with the same standard deviation.

All beads interact with each other via a spherical excluded volume potential, with the form of a truncated and shifted repulsive 12-6 Lennard-Jones pair potential with length parameter $\sigma_{ij}=\frac{1}{2}(\sigma_i+\sigma_j)$:

$$U_{LJ}(r_{ij})=\begin{cases} 4\epsilon\left[\left(\dfrac{\sigma_{ij}}{r_{ij}}\right)^{12}-\left(\dfrac{\sigma_{ij}}{r_{ij}}\right)^{6}+\dfrac{1}{4}\right], & r_{ij}<2^{1/6}\sigma_{ij} \\ 0, & r_{ij}\geqslant 2^{1/6}\sigma_{ij}. \end{cases} \quad (1)$$

Bead sizes σ_i specified by first calculating the gyration radii among atomic positions in each group, and then scaling these radii such that the volume of the repeat unit, accounting for the overlaps of adjacent beads, is equal to the van der Waals volume per repeat unit of BP-*A*-PC computed from experimental data using an equation-of-state analysis [28]. This yields a total volume fraction in the liquid of about 0.5. Values for $\sigma_i=4.49$, 5.19, 4.67 Å, respectively, for carbonate, isopropylidene, and phenylene beads. ϵ is chosen as the unit of energy, which we set at kT for our NVT molecular dynamics simulations, discussed in Sec. III.

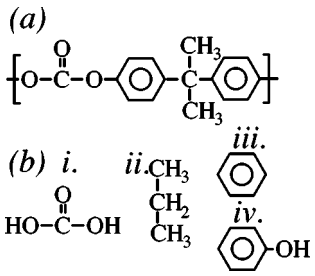

FIG. 4. (a) Chemical structure of the repeat unit BP-*A*-PC. (b) Analogous molecules used in the *ab initio* studies: (*i*) carbonic acid, (*ii*) propane, (*iii*) benzene, and (*iv*) phenol.

B. The dual-resolution model

The impetus for developing the dual-resolution model came directly from the Car-Parrinello simulations of phenol interacting with nickel, where we observed a strong dependence of the energy of interaction and interatomic forces on the angle of the C_1-C_4 vector relative to the surface normal. Including this dependence in a coarse-grained simulation is fundamentally impossible unless the level of resolution at the chain ends is increased. In the dual-resolution scheme, depicted in Fig. 2, the terminal carbonate (-O_b-CO_c-O_b-) groups are resolved atomistically. This results in the necessity to account for more intramolecular interactions than in the single-resolution case discussed above. Apart from these new interactions (discussed below), all aspects of the dual-resolution model are identical to those of the single-resolution model (presented above).

1. Specific surface interactions from Car-Parrinello DFT calculations

Ab initio DFT calculations, due to the accurate description of electronic properties, allow a realistic study of the interaction of molecules with metal surfaces. However, the large computational effort required confines this approach to the study of small systems. Keeping in mind this limitation, we developed a multiscale approach to simulate BP-*A*-PC on a Ni(111) surface [8], where the chemical unit of BP-*A*-PC was divided into comonomeric molecules small enough to study the interaction with the surface. The results from these calculations guided the development of the coarse-grained model. Specifically, we consider four molecules analogous to the comonomeric subunits of BP-*A*-PC (Fig. 4): carbonic acid (*i*), propane (*ii*), benzene (*iii*), and phenol (*iv*) representing, respectively, carbonate, isopropylidene, and phenylene (the last two) and study the interaction of each with a Ni(111) surface. We found that propane and carbonic acid

see the surface as a uniform hard wall. At an average distance of 3.2 Å, they experience significative repulsion, which strongly increases in magnitude below this distance. Hence, these molecules sample such distances at only vanishingly small probabilities.

Benzene and phenol experience strong adsorption energyies, respectively, 1.05 eV ($\approx 21kT$) and 0.91 eV at a center-of-mass distance ≈ 2 Å from the surface and in a horizontal orientation over the bridge site. Since the carbonate and isopropylidene show strong repulsion for distances shorter than 3.2 Å, *internal* phenylene is sterically forbidden by its neighbors to approach the surface to its ideal adsorption distance. Further studies of the interaction of benzene and phenol with the surface at larger distances show that the adsorption is short ranged and decays below 0.03 eV at a distance beyond 3 Å. Therefore, an *internal* phenylene comonomer has only a weak interaction with the surface.

The case is different for the chain-terminating phenoxy groups. Because the C_4-O_b torsional barrier is less than $1kT$ [30], a terminal carbonate can orient such that virturally no steric hindrance to the horizontal approach of the phenoxy end group to the surface exists. Thus, it is likely that *only* the chain-ends adsorb strongly to the surface (see Fig. 2). Previously, we incorporated the above information into a coarse-grained model of BP-*A*-PC melts next to a Ni(111) wall [8]. There we showed that the situation is dramatically different when the chain ends are preferentially attracted to the walls with respect to the case of an inert wall. In the dual-resolution model discussed here, we move from the ideal (optimal) flat adsorption to a more realistic description of the adsorption process by considering the interaction energy as a function of the angle θ formed by the carbon ring of the phenol with the surface (see Figs. 5 and 6). The dependence of phenol-nickel interaction energy on the phenol orientation is shown in Fig. 7, while details of the calculation are reported in the Appendix. Figure 7 shows that the interaction energy of phenol with a nickel surface is quite sensitive to its orientation. The goal of the dual-resolution model is to incorporate this sensitivity into the model of a liquid of entire BP-*A*-PC molecules interacting with nickel.

It is important to note that the potential energies predicted in these calculations do not account for dispersion forces. Thus, we have not attempted to model dispersive attractions between phenoxys and surface atoms in the coarse-grained model, as will be discussed in the following subsection. However, we do have confidence in the calculation's ability to account for the short-ranged behavior, including the strong sensitivities to distance and orientation. Because the energy scales of this short-ranged behavior is many kT, we must therefore treat these sensitivities in any reasonably accurate molecular model of BP-*A*-PC interacting with nickel. The short-ranged nature of the potential is the essential behavior that we captured and implemented in the classical coarse-grained potential used in this work.

2. Implementation

The bond between the outer of the two bridging oxygens (O_b) and the center of the phenoxy bead defines the C_1-C_4 orientation of the phenoxy group, relative to some external

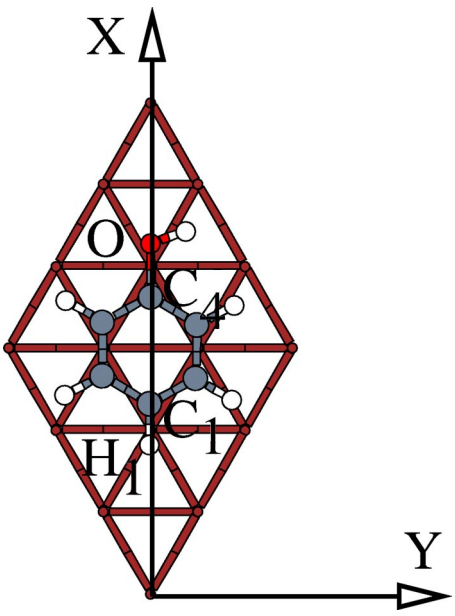

FIG. 5. Top view of the phenol molecule and surface top layer in the unit cell of simulation. The *x* axis divides the carbon ring into two symmetrical parts. The rotation is performed by pinning down the hydrogen H_1 (for the initial geometry) and rotating the molecule outward around the axis parallel to the *y* axis passing through H_1.

direction, as depicted in Fig. 2. We have chosen to keep the excluded volume representation of the resolved carbonates the same as all other carbonates; that is, the volume is carried by a sphere centered on the carbonate carbon, and only the orientations are resolved atomistically. The oxygens in the carbonate do not interact via any nonbonded interaction with any other atoms or beads in the system. Their only role is determining the intramolecular structure of the chain ends with sufficient detail to properly account for surface interactions. The bond angles and lengths in the resolved carbonates are enforced with simple harmonic potentials:

$$U_{\text{bond}}(r_{ij}) = \frac{1}{2} k_{ij} (r_{ij} - r_{ij}^0)^2, \tag{2}$$

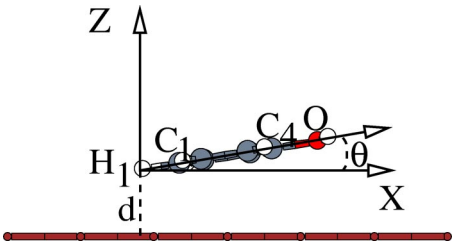

FIG. 6. Lateral view of the phenol molecule and surface top layer in the unit cell of simulation. When the rotation is performed H_1 is fixed at a distance $d = 2.0$ Å from the top layer of the surface, which is the equilibrium distance between the molecule and the surface, the molecule is then rotated in the *xz* plane of an angle θ. During the geometry optimization the *z* coordinates of the carbons are fixed, while all the other degrees of freedom are allowed to relax; this allow us to have the carbon ring at a fixed angle with respect to the surface and to avoid transversal rotations.

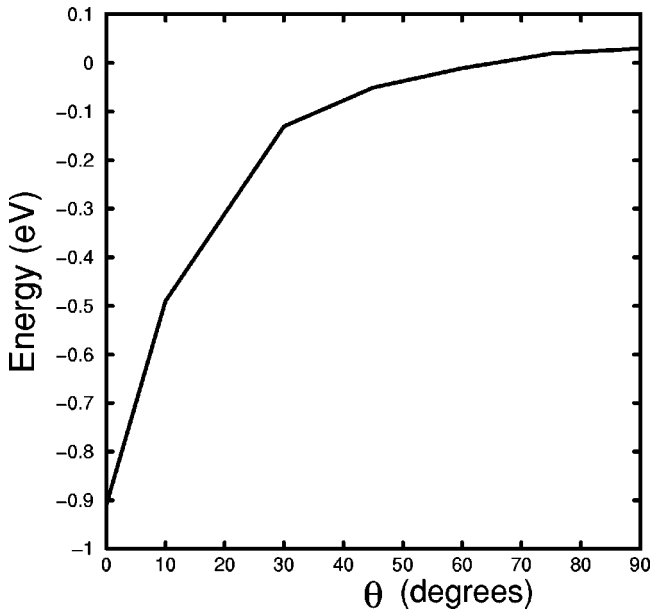

FIG. 7. Phenol-nickel interaction energy as a function of phenol orientation angle θ, as defined in Fig. 6.

$$U_{\text{angle}}(\theta_{ijk}) = \frac{1}{2} k_{ijk}(\theta_{ijk} - \theta^0_{ijk}). \tag{3}$$

The two C-O_b bonds have $r^0 = 1.33$ Å and $k = 2.6kT/\text{Å}^2$. The C-O_c bond has $r^0 = 1.16$ Å and $k = 2.6kT/\text{Å}^2$. Angles at the O_b have $\theta = 121.44°$ and $k = 0.054kT/\text{deg}^2$, the O_b-C-O_b angle has $\theta = 108°$ and $k = 0.054kT/\text{deg}^2$, and the two O_c-C-O_b angles have $\theta = 126°$ and $k = 0.054kT/\text{deg}^2$ [29].

The two torsions ϕ (one for each C-O_b bond) are subject to potentials taken from standard molecular mechanics simulations of BP-*A*-PC [29]:

$$U_{\text{torsion}}(\phi) = \frac{1}{2} k_1[1 - \cos n_1(\phi - \phi_0)] + \frac{1}{2} k_2[1 - \cos n_2(\phi - \phi_0)], \tag{4}$$

where $k_1 = 3.2kT$, $n_1 = 2$, $k_2 = 0.84kT$, $n_2 = 2$, and $\phi_0 = 180°$.

Additional components of the intramolecular description of the dual-resolution model account for the ''interface'' between the atomistic terminal carbonates and the coarse-grained remainder of the chain. Here, we make use of the notation illustrated in Fig. 2, in which coarse-grained beads are denoted by lower-case letters, and atoms by upper-case letters. The atomistic carbonate groups are connected to the rest of the chains by bonds between the bridging oxygens (O_b) and the neighboring *internal* phenylene bead and phenoxy chain end. These two bonds are treated with a harmonic potential identical in form to Eq. (2), with $k = 2.6kT/\text{Å}^2$ and $r^0 = 2.76$ Å. Furthermore, the c-i_t-c_t bond angle potential is not applied in exactly the same manner as all other internal c-i-c bond angles. Because we have exact knowledge of the location of the terminal carbonate's carbon, the only uncertainty that would require a distribution-function description of the bond angle is due to the internal carbonate. Hence, for the c-i_t-O_b bond angle, we use a Boltzmann-inverted potential from a probability distribution that samples the c-i_t-O_b bond angle at $T = 570$ K, in the same manner as the c-i-c and i-c-i distributions were created. This distribution is also given in Fig. 3.

The remaining components of the dual-resolution model deal with bead-wall interactions. We imagine a simulation system representing a slit pore of width L, with the walls normal to the z direction, and periodic boundary conditions in x and y. The ''left'' wall originates at $z = Z_L$, and the ''right'' wall at $z = Z_R$, where $Z_L < Z_R$. Furthermore, depending on the type of bead, the walls are represented either by a one-dimensional repulsive potential, or as an array of sites in a hexagonal (111) arrangement, with lattice spacing a_0.

All internal beads interact with the walls via a one-dimensional 10-4 repulsive potential:

$$U_{w,rep}(z) = U_{10\text{-}4}(z - Z_L) + U_{10\text{-}4}(Z_R - z), \tag{5}$$

$$U_{10\text{-}4}(z) = \begin{cases} 2\pi\epsilon_w\sigma_w^2\left[\frac{2}{5}\left(\frac{\sigma_w}{z}\right)^{10} - \left(\frac{\sigma_w}{z}\right)^4 + \frac{3}{5}\right], & z < \sigma_w \\ 0, & z \geqslant \sigma_w . \end{cases} \tag{6}$$

The value of σ_w for each type of bead was taken from *ab initio* calculations, as discussed elsewhere [8]. These calculations demonstrated that isopropylidene and carbonate subunits are repelled from nickel for all relevant distances. Although isolated benzene and phenol will strongly adsorb on nickel, the geometry of the repeat unit sterically hinders adsorption of *internal* phenylenes. Hence, we choose the (ϵ_w, σ_w) of both isopropylidenes and carbonates such that each bead experienced $1kT$ of repulsive energy at a distance of $0.9\sigma_w$. A short test calculation showed that internal phenylenes will not approach the surface close enough to attractively interact; hence, attractive surface interactions of internal phenylenes are not included.

For each *terminal* phenoxy group i, the following surface interaction potential is applied:

$$U_{i,\text{or}} = \sum_{\text{site}j} U_{\text{site}}(r_{ij}), \tag{7}$$

where index j runs over the arrays of (111) sites (with a Ni-Ni nearest neighbor distance of 2.51 Å) on both walls, and

$$U_{\text{site}}(r_{ij}, \theta_i) = \begin{cases} 4\left[\left(\frac{\sigma_{ij}}{r_{ij}}\right)^{12} - \left(\frac{\sigma_{ij}}{r_{ij}}\right)^6 + \frac{1}{4}\right] - \epsilon(\theta_i), & r_{ij} < r_0 \\ \frac{1}{2}\epsilon(\theta_i)\left[\cos\left(\pi\frac{r_c - r_{ij}}{r_c - r_0}\right) - 1\right], & r_0 < r_{ij} \leqslant r_c \\ 0, & r_{ij} \geqslant r_c , \end{cases} \tag{8}$$

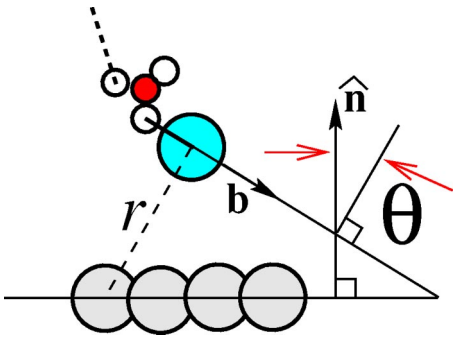

FIG. 8. Illustration of the orientation dependent surface interaction for terminal phenoxy groups in the dual-resolution model. θ is the inverse sine of the angle defined by the C_1-C_4 orientation (vector **b**) and the surface normal $\hat{\mathbf{n}}$.

where $r_0 = 2^{1/6}\sigma_{ij}$, and r_c is a desired cutoff. θ_i describes the orientation of the phenoxy ring, as described previously. In specific terms, θ_i measures the orientation of the bond between the outer O_b of the terminal carbonate and the center of the ith terminal phenoxy, $\mathbf{b}_i$, (i.e., the C_1-C_4 orientation) relative to the surface normal $\hat{\mathbf{n}}$, as depicted in Fig. 8:

$$\theta_i = \arcsin\frac{\mathbf{b}_i \cdot \hat{n}}{b_i}, \tag{9}$$

Note that $\hat{\mathbf{n}} = \hat{z}$ for the left wall, and $\hat{\mathbf{n}} = -\hat{z}$ for the right wall. $\epsilon(\theta_i)$ is an empirical function that describes the orientational dependence of the well depth of the attractive interaction:

$$\epsilon(\theta_i) = \exp\left(-\alpha\frac{\sin^2\theta_i}{1-\sin^2\theta_i}\right). \tag{10}$$

For the simulations discussed here, we used $r_0 = 2.0$ Å, $r_c = 2.7$ Å, $\epsilon_0 = 6.0kT$, and $\alpha = 10.0$. Representative plots of $U_{\text{site}}(r_{ij}, \theta_i)$ and $\epsilon(\theta_i)$ are shown in Fig. 9. It can be seen from Fig. 9(b) that the absolute value of the well depth strongly decreases with increasing orientational angle θ_i; at an orientation of 45° for the decay parameter $\alpha = 10$, there is essentially no attraction to the surface. This potential was chosen to closely resemble the situation as given by the *ab initio* calculations. The interaction has to be short ranged and take the angular constraints properly into account. The latter is needed in order to reproduce the effect of the adsorption onto the chain conformation near the surface. The adsorption energy on the coarse-grained level was chosen significantly lower than given by the *ab initio* calculations ($6kT$ instead of about $20kT$). The reason for this is that, given the spacing of the surface atoms, phenoxy beads interact with an average of three surface atoms simultaneously. The total interaction of a phenoxy with surface is the sum of all phenoxy-surface atom interactions, and the parameters define a single phenoxy-surface atom interaction. Therefore, the strength of the single phenoxy-surface atom interaction must be roughly one-third of the predicted value. Moreover, we assume that ≈ 1–$2\,kT$ of energy is used to overcome the roughly $1kT$ rotational energy barrier around the C_4-O_t bond to allow the

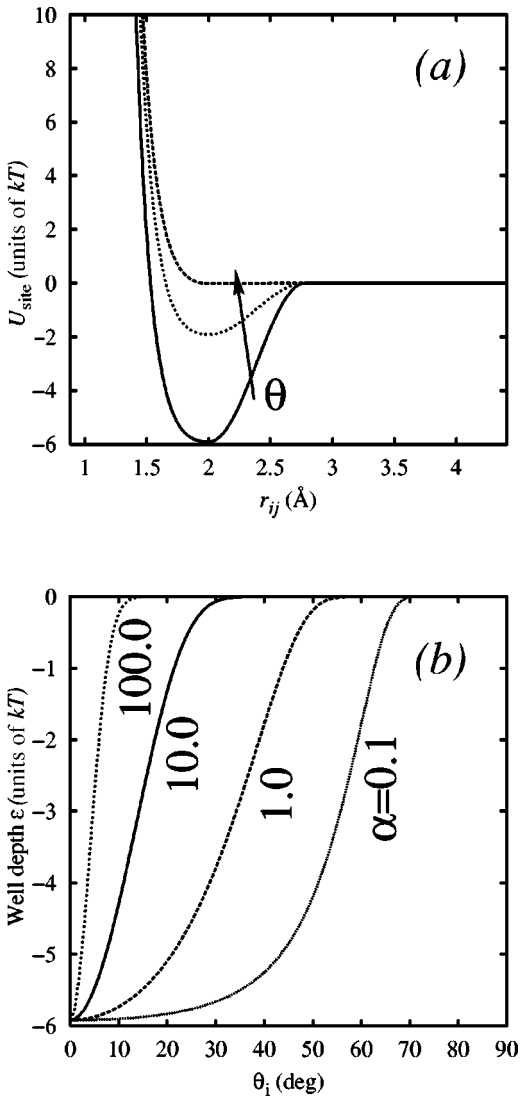

FIG. 9. (a) Surface site interaction U_{site} for increasing values of orientation angle θ_i ($\theta_i = 0°$, 10°, and 60° shown) with strength parameter $\alpha = 10.0$ and (b) orientation dependent well depth $\epsilon(\theta_i)$ for various values of strength parameter α.

phenoxy ring to approach a horizontal orientation. Thus, the potential used in the coarse-grained simulations should allow for a *maximum* phenoxy-surface interaction energy of about $18kT$. As will be discussed later in this paper, this maximum adsorption energy is not achieved on average by phenoxy chain ends in a melt of chains next to a nickel surface.

As alluded to above, we do not explicitly consider the transverse orientation of the terminal phenoxy groups. The transverse orientation is defined by a vector **t** perpendicular to the C_1-C_4 direction (which we call **b**) lying in the plane of the ring. Both **b** and **t** must be perpendicular to $\hat{\mathbf{n}}$ in order for the phenoxy ring to be parallel to the surface plane. As mentioned already, recent atomistic molecular dynamics (MD) simulations [21,29,30] assume that the torsions which govern the orientation of the vector **t**, (the torsions of the O_b-C_1 bond) have barriers of about $1kT$ at our temperature of interest. This $1kT$ penalty that is potentially paid during this

reorientation is hardly significant compared to the $\sim 20kT$ gain by adsorbing the phenolic chain end, meaning that we expect transverse reorientation of the phenolic chain end to happen ''instantaneously.'' However, the orientation along the chain direction must respond to both the attraction of the surface and the connectivity of the chain. Therefore, it is of much greater importance that the C_1-C_4 direction is properly accounted for.

III. MOLECULAR DYNAMICS SIMULATION DESCRIPTION

Coarse-grained samples

Molecular dynamics simulation was performed using the model above in order to examine the structure of the BP-*A*-PC–Ni interface. The velocity-Verlet algorithm was used to integrate the particle equations of motion using a constant time step of 0.005 τ. A Langevin-type thermostat with friction $\Gamma = 0.5\ \tau^{-1}$ was used to keep the temperature constant at 1.0 [31]. Reduced Lennard-Jones units were used throughout, where the length conversion factor S is 4.41 Å/σ.

Liquid samples were generated by first specifying number of chains and number of repeat units per chain, and the system density. Chains were then randomly placed in a box and grown according to the bond length and bond angle probability constraints; for details, see Ref. [6]. A 5000-step ''push-off'' integration is then performed to remove bead-bead overlaps [32]. During this stage, all particles interact via a radially shifted Weeks-Chandler-Anderson repulsive particle-particle pair potential,

$$U_{\mathrm{rs}}(r_{ij}) = \begin{cases} 4\epsilon\left[\left(\dfrac{\sigma_{ij}}{r_{ij}+2^{1/6}\sigma_{ij}b(t)}\right)^{12} - \left(\dfrac{\sigma_{ij}}{r_{ij}+2^{1/6}\sigma_{ij}b(t)}\right)^{6} + \dfrac{1}{4}\right], & [r_{ij}+2^{1/6}\sigma_{ij}b(t)] < 2^{1/6}\sigma_{ij} \\ 0, & [r_{ij}+2^{1/6}\sigma_{ij}b(t)] \geqslant 2^{1/6}\sigma_{ij}, \end{cases} \tag{11}$$

where $\sigma_{ij} = \frac{1}{2}(\sigma_i + \sigma_j)$ and $\epsilon = 1kT$. The radial shift term $b(t)$ decays linearly from unity to zero over the duration of the push-off stage:

$$b(t) = \frac{t_f - t}{t_f - t_i}.$$

Here, t_i and t_f are the initial and final time values of the push-off stage, respectively.

The sample consisted of 240 chains of ten repeat units each. This corresponds to 49 beads per chain in dual-resolution scheme. The system density was fixed at 1.05 g/cc, corresponding to the experimental system density at 570 K. The box dimensions (x,y,z) were 98.0, 95.8, and 110.8 Å, respectively. The dimensions in x and y are set to accomodate a (111) hexagonal lattice constructed from orthohexagonal (rectangular) unit cells with a nearest neighbor distance of 2.51 Å. These dimensions correspond to 36 cells in the x direction, and 22 in y, with two sites per cell, for a total of 1584 sites per wall.

After the push-off phase, a second simulation phase is performed to ''turn on'' the walls. Here, the z periodicity of the simulation box is turned off, leaving the beads with absolute, ''unfolded'' z positions. The wall potentials are then applied such that the origins, Z_L and Z_R in Eq. (5), were placed one bead diameter beyond the two beads having extremal z positions; in other words, the wall origins were placed as close to each other as possible, while containing all beads in the system. The walls are then incrementally brought closer together over about 5000 steps. The criteria for stopping the wall movement is that the bulk density far from the walls matches the bulk density from the fully periodic simulation cell. After the desired density in the bulk region was established, we observed that the wall-to-wall separation was about 110 Å. During this warm up, *all* particles interact with the wall as if it were featureless. At this point, the full MD simulation is begun, in which the phenoxy end particles interact with the individual sites on the walls via the previously described orientation dependent potential.

IV. RESULTS AND DISCUSSION

A. Dynamics

Before discussing the results from the simulation in the slit pore, we present a brief discussion of results from a bulk run, for purposes of comparison. In Fig. 10, we present the mean-squared displacements g_1, g_2, and g_3 for the funda-

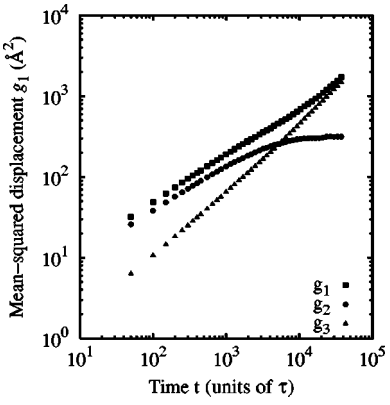

FIG. 10. Bulk mean-squared displacements for $n = 10$ BP-*A*-PC, computed via MD simulation of the fundamental 4:1 coarse-grained model (no end resolution).

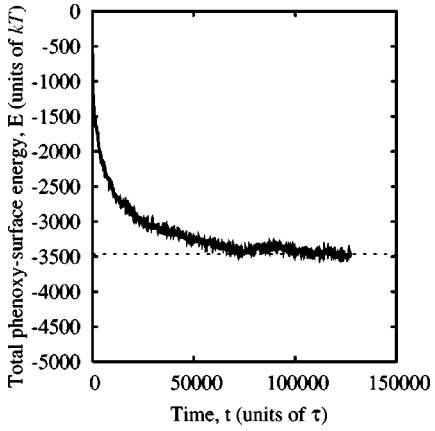

FIG. 11. Phenoxy-surface interaction energy versus time. The dashed line indicates the achieved equilibrium value.

mental 4:1 model chains (with no end resolution) from a bulk simulation of 80 chains of ten repeat units each. g_1 is the mean-square displacement of the inner five monomers of each chain, g_2 is the mean-squared displacement of these monomers relative to the chain's center of mass, and g_3 is the mean-squared displacement of the chain centers of mass. From the point at which g_2 and g_3 cross, which indicates roughly the average time required for a chain to diffuse a distance equal to its own radius of gyration, we infer an equilibration time of roughly 6000τ.

Turning now to the confined system, the first result we consider is the total energy of the phenoxy-wall interactions vs time, shown in Fig. 11. We observe that the time to equilibrate this energy, roughly $70\,000\tau$, is more than ten times longer than the characteristic relaxation time of $n=10$ BP-*A*-PC from our previous calculations. This slow relaxation has its origin in a large slowing down of monomer motion next to the surface, mainly due to the site-specific nature of the surface interaction. This is demonstrated by Fig. 12, in which we show the mean-square displacements g_1 for monomers in two different regions. Region I is less than

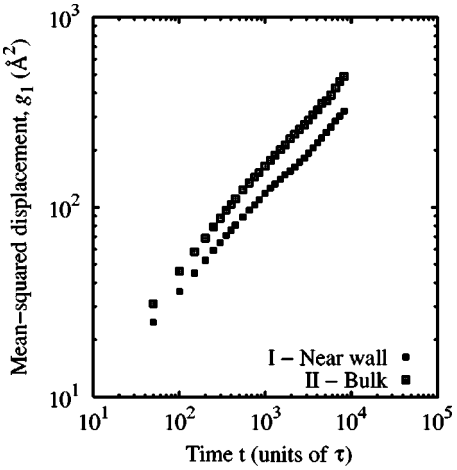

FIG. 12. Mean-squared displacements g_1 in the confined system, segregated by position of the origin of each particle: zone I if $z_0<40$ Å, zone II otherwise.

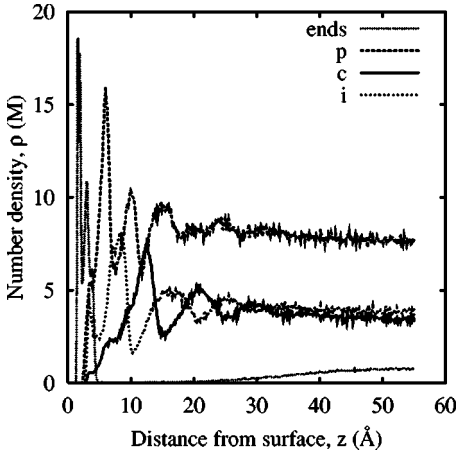

FIG. 13. Bead depth profiles (number density versus distance from surface) of coarse-grained beads over the entire width of the slit pore. Mirror image symmetry about the center line is enforced. For this plot, each chain end (carbonate plus terminating phenoxy) is counted as a single particle. Shown are the profiles for internal phenylenes (p), carbonates (c), and ispropylidenes (i).

40 Å from either wall, and Region II is the middle 25 Å. These mean-squared displacements were computed over the final $10\,000\ \tau$ of the simulation, during that time no change in the surface energy could be observed. Of course, these displacements near the wall are the result of a rather large fluctuations, since the displacement of the bonded chains are much smaller than those of the nonbonded chains. However, as will be shown below, most chain in the ''surface region'' have at least one link to the surface. As a consequence, we observe from these two sets of mean-square displacements that significant slowing down occurs next in the region nearer the walls. This is not surprising, because chain ends are essentially fixed on the surface, causing entire chains in this region to become immobilized. Over this short time window, however, we do not observe a saturation of g_1.

B. Structure

From bulk simulations, we know that the root-mean-squared radius of gyration of $n=$ ten repeat unit chains of our fundamental 4:1 BP-*A*-PC is about 20.5 Å. This length scale figures prominently in nearly all aspects of the liquid structure next to the walls. We first consider the number density of beads as a function of distance from the walls, z. Figure 13 shows these profiles for the internal phenylene, carbonate, and isopropylidene beads, as well as the profile for chain ends (carbonate plus phenoxy), each counted as a *single* particle. We see an unusually large amount of structure in these profiles, with significant layering in the density out to a depth of about one $\langle R_g^2\rangle^{1/2}$. Interestingly, the alternating nature of the chain sequence is revealed in the alternating layering of isopropylidenes and carbonates out to this distance: where ispropylidene density is high, carbonate density is low, and vice versa, with peaks in the linking phenylene density at depths where the carbonate and isopropylidene densities are equal. Also, chain ends are strongly localized at the surface, as expected. Unexpected, however, is the obser-

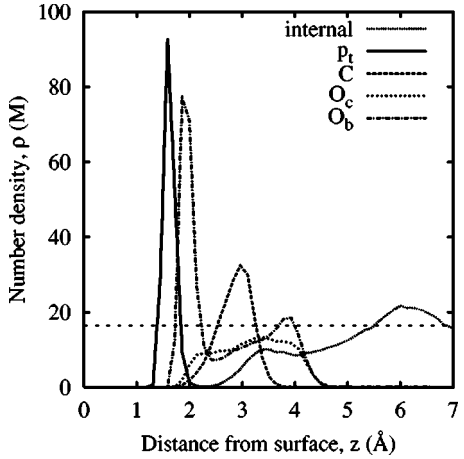

FIG. 14. Bead depth profiles near the surface, resolved to show components of the chain ends. For this plot, all internal beads are lumped into a single curve. The dashed line shows the expected bulk number density. Shown are the profiles for terminating phenoxys (p_t), terminating carbonate carbon (C), terminating carbonate bridging oxygens (O_b), terminating carbonate lone oxygen (O_c), and the lumped profile for internal beads.

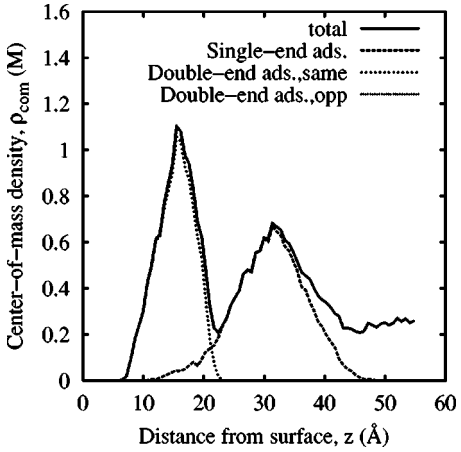

FIG. 15. Chain center-of-mass depth profiles, showing division into populations of chains which adsorb both ends on a surface, one end on the surface, and no ends on the surface.

vation of a zone strongly depleted in end groups which reaches a full $2\langle R_g^2\rangle^{1/2}$ into the liquid. Clearly, equilibrium conformations characteristic of bulk BP-*A*-PC are not responsible for this compositional behavior.

In Fig. 14, we show a close up of the density profile near the surface, resolving the individual atoms in the terminal carbonate groups. Here, the angular dependence of phenoxy-nickel interaction energy causes a strong correlation between the location of terminal phenoxy centers and bridging oxygens. The intensity of the phenoxy peak indicates that, at equilibrium, 290 out of 480 ends are adsorbed, with an average energy of $12kT$ each [33]. We see that, on average, the maximum adsorption energy is not achieved, demonstrating a competition between entropies of chain configurations and packing, and surface attraction.

We now consider the likelihood of end adsorption as a function of distance from the surface. In Fig. 15, we show the center-of-mass density profile $\rho_{\mathrm{COM}}(z)$ divided into two major categories: those chains with both ends adsorbed and those chains with only one end adsorbed. Also the total density of chain centers of mass is given. (The profile for chains with no ends adsorbed are not shown explicitly.) These profiles shown in Figs. 13 and 15, reveal the nature of two depletion scenarios, which are closely interconnected. First, there is a large zone of depletion of chain ends, as discussed before, as a consequence of this $\rho_{\mathrm{COM}}(z)$ displays two distinct layers: in the layer nearest to the surface, any chain with a center of mass in this layer has both ends adsorbed on the surface. This layer extends about one $\langle R_g^2\rangle^{1/2}$ into the liquid. The next layer out, again about one $\langle R_g^2\rangle^{1/2}$ in width, contains a large majority of chains with a single-end adsorbed. Beyond $2\langle R_g^2\rangle^{1/2}$, there exist only very few chains with a single-end adsorbed. To study such effects quantitatively longer chains are needed. Of course, no chain exists in a state with each end adsorbed to opposite walls. The existence of the end-attractive surface, together with the constraints of dense packing in the liquid, gives rise to this unique structure, which we did not find reported elsewhere.

Finally, we assess the consequences of the above structure on the internal structure of the chains, measured by the lab-frame components of the gyration tensors $\langle R_{g,\alpha\alpha}^2\rangle$ where $\alpha\alpha \in \{xx,yy,zz\}$. $\langle R_{g,\alpha\alpha}^2\rangle$ as a function of distance from the walls is shown in Fig. 16. Again, we see strong effects on the structure up to a depth of about $2\langle R_g^2\rangle^{1/2}$. Considering the two layers defined above, in the layer closest to the wall, chains are significantly compressed in the *z* direction. This behavior can arise in any dense polymer systems in the absence of end attraction to the surface, as has been seen in previous simulations of bead-spring chains [34,35]. This effect is mainly due to the orientation of the gyration tensor near the surface. However, in the region $\langle R_g^2\rangle^{1/2} < z < 2\langle R_g^2\rangle^{1/2}$, we see that chains are strongly deformed, displaying significant elongation in the *z* direction. The magnitude of this stretching can be appreciated by noting that the maximum value of the *z* component of the mean-squared

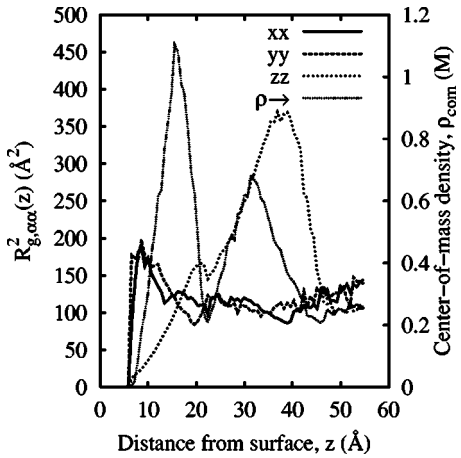

FIG. 16. Depth profiles of chain lab-frame gyration radius components $\langle R_{g,\alpha\alpha}^2\rangle$. Plotted against the right-hand *y* axis is the center-of-mass number density profile.

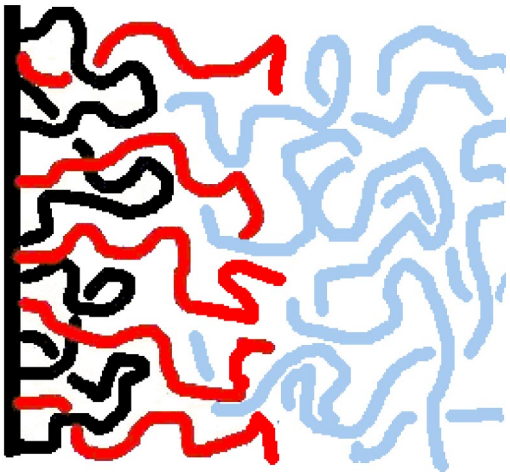

FIG. 17. Cartoon of the average chain conformations near the surface. Since the chains are relatively short and only the chain ends adsorb, there is no entanglement network, which would otherwise enhance the bulk adhesion to the surface. Black lines represent chains with both chain ends stuck to the surface, dark gray lines represent chains with only one chain end stuck to the surface and the other in the bulk, and light gray lines represent chains in the bulk.

radius of gyration profile $\langle R^2_{g,zz}\rangle(z)$ is greater than $3\langle R^2_{g,\mathrm{bulk}}\rangle$. These are the chains that have adsorbed a single end on the surface, but are restricted from adsorbing the other end due to dense packing of the doubly adsorbed chains near the wall. This exclusion effect acts to localize chain centers of mass in this region. Possible similarities in the conformations of these chains to polymer brushes will be of interest in the case of longer polymers.

The simulation results provide us with a clearer picture of how the molecules arrange at the interface, which we depict in Fig. 17. This arrangement is characterized by the localizing of chain centers of mass in two distinct layers, $0<z<\langle R^2_g\rangle^{1/2}$ (layer I) and $\langle R^2_g\rangle^{1/2}<z<2\langle R^2_g\rangle^{1/2}$ (layer II) relative to the surface. Chains near the surface are compressed in the direction normal to the surface, while chains in layer II are strongly stretched in this direction. This results from a competition between energetic end adsorption and entropic packing in the dense liquid. For the present short chains, though the chain ends adsorb (almost) irreversibly, we expect that this leads only to a rather weak adhesion to the bulk polymer matrix, because chains with both ends stuck are not likely to be significantly entangled with the bulk chains. Simulations of longer chains are in progress to examine this effect.

V. CONCLUSIONS AND OUTLOOK

We have presented a dual-resolution coarse-grained model of bisphenol-*A*-polycarbonate, which allows molecular simulation of dense liquids next to nickel surfaces. The essential feature of this model is that the ends of the polymer chains adsorb strongly to the surface, when the ends are aligned horizontally. The model accounts for this effect, while simultaneously accounting for the configurational statistics of the chains. From a large MD simulation of short BP-*A*-PC chains of ten repeat units in a slit-pore geometry formed by (111) nickel walls, we observe strong effects on the liquid structure due to this adsorption.

Many interesting questions about the behavior of BP-*A*-PC, in particular, and polymers, in general, next to metal surfaces arise from this work. We are faced by the special situation that only the chain ends strongly bind to the surface. This is due to the fact that the inner phenylene rings are excluded from binding to the surface due to steric effects. It would be very interesting to consider similar questions for other synthetic and biological macromolecules, and whether such effects can be utilized to facilitate certain properties and/or functions, e.g., specific adhesion, binding, and recognition. This will be an important aspect of future studies. Also important for future work is experimental observation of chain-end adsorption, which so far has not been reported.

Another related topic is the dependency of the glass transition temperature in thin (supported) films. There is a fairly large current literature on the problem of lowering, and in some cases, raising the glass transition temperature compared to bulk samples. (See, e.g., Ref. [36]). In the latter case, one expects a crucial dependence on the specific support surface polymer interactions.

Of current primary importance is to understand how strongly this behavior scales with chain length. In experiment, one typically deals with polydisperse samples. For entropic reasons, the shorter chains prefer to aggregate near the surface compared to the longer chains. Thus, we expect that the present scheme qualitatively is applicable to experimental-technical samples as well. Because BP-*A*-PC molecules are relatively stiff, it is also of interest to consider whether such a two-layer structure would arise in systems of more flexible chains with preferred end adsorption.

ACKNOWLEDGMENTS

We are grateful to M. Parrinello for helpful suggestions and for providing us the CPMD code, and to F. Müller-Plathe and A. Alavi for helpful comments and suggestions. This work was supported by the BMBF, under Grant No. 03 N 6015, and the Bayer Corporation.

APPENDIX

In this appendix, we report technical details of the *ab initio* calculations for determining the angular-dependent potential between phenol and the Ni surface. An extended description of the calculations done for carbonic acid, propane, benzene and phenol will be presented in a forthcoming publication [37]. We use the CPMD code [38] in the FEMD version of Alavi [39,40]. In this version, the electron density and the Hellman-Feynmann forces are computed self-consistently using a subspace diagonalization of the high temperature matrix. The subspace is expanded in a plane-wave basis set with a cut off of 60 Ry. *k*-point sampling of the electronic states in the Brillouin zone of the supercell is implemented, and a partial occupation of states at the Fermi level can be handled.

The system consists of a phenol molecule and a Ni(111) surface. The latter is represented by four close-packed layers of Ni(111) (lattice parameter $b_0 = 3.543$ Å) with the two bottom layers fixed and the top two allowed to relax. We use a (3×3) lateral supercell of hexagonal symmetry and employ a $3\times3\times1$ *k*-point mesh. The cell dimension in the direction normal to the surface is 20 Å so that the minimum thickness of the vacuum between the phenol molecule and the bottom layer of the image slab of Ni(111), i.e., in the configuration where the phenol is perpendicular to the surface, is about 7 Å. This is more than the thickness of the Ni film considered. For carbon and oxygen, a Troullier-Martins pseudopotential [41] is used, while a local pseudopotential is used for hydrogen [42], and the pseudopotential developed by Lee is used for nickel [43]. We use the Perdew-Burke-Ernzerhof [44] generalized gradient approximation. This technical setting was tested by calculating nickel bulk properties, surface properties, and phenol geometrical properties and checking the agreement with previous work and experiments [45,46].

We found that the most energetically favorable configuration is the one with the carbon ring of the phenol lying parallel to the surface over the bridge site at an average distance from the surface of about 2.0 Å; this corresponds to an adsorption energy of 0.91 eV. In order to calculate the interaction energy as a function of the angle θ between the carbon ring of the phenol and the surface, we performed BFGS geometry optimization for several initial geometries corresponding to different values of θ, which is kept fixed during the relaxation process. We set the system in a way that in the optimal flat configuration the *x* axis bisects the carbon ring in two symmetrical parts in the *xy* plane passing through the oxygen. The rotation is then performed in the *xz* plane by pinning the hydrogen H1, diametrically opposed to the oxygen, at a distance of 2.0 Å, corresponding to the equilibrium distance, (see Figs. 5 and 6). This means that in order to keep θ fixed and to avoid transverse rotations during the *ab initio* geometry optimization, we simply need to keep fixed the *x* and *z* coordinates of the carbons; all the other degrees of freedom can be allowed to relax (see Fig. 6). We should also say that, in general, for a a given angle θ rotations in the *yz* plane around the *x* axis leads to a weaker attraction due to the strong repulsion of the hydrogens, which allowed us to neglect, in first approximation, transverse rotations.

[1] J. Baschnagel, K. Binder, P. Doruker, A.A. Gusev, O. Hahn, K. Kremer, W.L. Mattice, F. Müller-Plathe, M. Murat, W. Paul, S. Santos, U.W. Suter, and V. Tries, Adv. Polym. Sci. **152**, 41 (2000).

[2] W. Paul, K. Binder, K. Kremer, and D.W. Heermann, Macromolecules **24**, 6332 (1991).

[3] K. Kremer and F. Müller-Plathe, MRS Bull. **26**, 205 (2001).

[4] F. Müller-Plathe, ChemPhysChem **34**, 2335 (2002).

[5] W. Tschöp, K. Kremer, O. Hahn, J. Batoulis, and T. Bürger, Acta Polym. **49**, 75 (1998).

[6] W. Tschöp, K. Kremer, J. Batoulis, T. Bürger, and O. Hahn, Acta Polym. **49**, 61 (1998).

[7] O. Hahn, L. Delle Site, and K. Kremer, Macromol. Theory Simul. **10**, 288 (2001).

[8] L. Delle Site, C.F. Abrams, A. Alavi, and K. Kremer, Phys. Rev. Lett. **89**, 156103 (2002).

[9] C.F. Abrams and K. Kremer, Macromolecules **36**, 260 (2003).

[10] L. Morbitzer and U. Grigo, Angew. Makromol. Chem. **162**, 87 (1988).

[11] A.F. Yee and S.A. Smith, Macromolecules **14**, 54 (1981).

[12] D. Schaefer, M. Hansen, B. Blümich, and H.W. Spiess, J. Non-Cryst. Solids **131-133**, 777 (1991).

[13] G. Floudas, J.S. Higgins, G. Meier, F. Kremer, and E.W. Fischer, Macromolecules **26**, 1676 (1993).

[14] F. Weigand and H.W. Spiess, Macromolecules **28**, 6361 (1995).

[15] R. Wimberger-Friedl and H.F.M. Schoo, Macromolecules **29**, 8871 (1996).

[16] L. Li and A.F. Yee, Macromolecules **35**, 425 (2002).

[17] J.H. Shih and C.L. Chen, Macromolecules **28**, 4509 (1995).

[18] C.F. Fan, C. Tahir, and W. Shi, Macromol. Theory Simul. **6**, 83 (1997).

[19] S.F. Tsai, I.K. Lan, and C.L. Chen, Comput. Theor. Polym. Sci. **8**, 283 (1998).

[20] J.T. Bendler, Comput. Theor. Polym. Sci. **8**, 83 (1998).

[21] P. Ballone, B. Montanari, R.O. Jones, and O. Hahn, J. Phys. Chem. A **103**, 5387 (1999).

[22] P. Robyr, Z. Gan, and U.W. Suter, Macromolecules **31**, 6199 (1998).

[23] M. Utz, P. Robyr, and U.W. Suter, Macromolecules **33**, 6808 (2000).

[24] L.J. Fetters, D.J. Lohse, S.T. Milner, and W.W. Graessley, Macromolecules **32**, 6847 (1999).

[25] J.S. Shaffer, A.K. Chakraborty, M. Tirrell, H.T. Davis, and J.L. Martins, J. Chem. Phys. **95**, 8616 (1991).

[26] A.K. Chakraborty, J.S. Shaffer, and P.M. Adriani, Macromolecules **24**, 5226 (1991).

[27] J.S. Shaffer and A.K. Chakraborty, Macromolecules **26**, 1120 (1993).

[28] I.C. Sanchez and J. Cho, Polymer **36**, 2929 (1995).

[29] H. Meyer, O. Hahn, and F. Müller-Plathe, J. Phys. Chem. B **103**, 10 591 (1999).

[30] O. Hahn, D.A. Mooney, F. Müller-Plathe, and K. Kremer, J. Chem. Phys. **111**, 6061 (1999).

[31] K. Kremer and G.S. Grest, J. Chem. Phys. **92**, 5057 (1990).

[32] C.F. Abrams and K. Kremer, J. Chem. Phys. **115**, 2776 (2001).

[33] Note that the optimal adsorption site in the coarse-grained description of the surface corresponds to the center of the equilateral triangle, whose vertices are three interacting sites of the surface. Note also that the the coarse-grained surface only reflects the basic geometrical properties of the real surface, but they are not identical.

[34] I. Bitsanis and G. Hadziioannou, J. Chem. Phys. **92**, 3827 (1990).

[35] D.Y. Yoon, M. Vacatello, and G.D. Smith, in *Monte Carlo and Molecular Dynamics Simulations in Polymer Science*, edited by K. Binder (Oxford University Press, Oxford, 1995).
[36] S. Herminghaus, K. Jacobs, and R. Seemann, Eur. Phys. J. E **5**, 531 (2001).
[37] L. Delle Site, A. Alavi, and C. F. Abrams (unpublished).
[38] J. Hutter, A. Alavi, T. Deutsch, M. Bernasconi, S. Goedecker, D. Marx, M. Tuckerman, and M. Parrinello, Computer Code CPMD Version 3.4.1 (Max-Planck-Institut für Festkörperforschung and IBM Zurich Research Laboratory, 1999).
[39] A. Alavi, J. Kohanoff, M. Parrinello, and D. Frenkel, Phys. Rev. Lett. **73**, 2599 (1994).
[40] A. Alavi, in *Monte Carlo and Molecular Dynamics of Condensed Matter Systems*, edited by K. Binder and G. Gallavotti (Italian Physical Society, Bologna, 1996), Chap. 25, p. 649.
[41] N. Troullier and J.L. Martins, Phys. Rev. B **43**, 1993 (1991).
[42] F. Gygi, Phys. Rev. B **48**, 11 692 (1993).
[43] M.H. Lee, Ph.D. thesis, Cambridge University, 1995.
[44] J.P. Perdew, K. Burke, and M. Ernzerhof, Phys. Rev. Lett. **77**, 3865 (1996).
[45] G. Kresse and J. Hafner, Surf. Sci. **459**, 287 (2000).
[46] Benedito José Costa Cabral, René Gil Bakker Fonseca, and José Artur Martinho Simões, Chem. Phys. Lett. **258**, 436 (1996).